Measurement Issues in the Characterization of Ferrite Magnetic Material

Glenn R. Skutt Fred C. Lee
Bradley Dept. of Electrical Engineering
Virginia Tech
Blacksburg, Va 24061-0111

John G. Breslin
Power Electronics Research Centre
Dept. of Electronic Engineering
University College, Galway, IRELAND

Abstract - **Ferrites have been examined in great detail since they were first introduced in the middle of the century, and standardized material data sheets are widely available. While these test data are particularly useful in a common applications, there are still areas where the available material information is lacking. In particular, in order to evaluate the dimensional effects encountered in some larger cores it is important to have information not only on the permeability and loss density of the core but also on the electrical conductivity and dielectric constant—or permittivity—of the material. This paper reviews measurement techniques for determining ferrite material characteristics and illustrates the impact of winding location and sample size on the measured material characteristics.**

I. INTRODUCTION

As power conversion circuits continue to evolve, there is an increased need for reliable data on the magnetic materials used to construct the transformers and inductors used in high-frequency, high-power circuits. Such circuits require magnetic components with large magnetic core structures. However, since the material data available in core manufacturer's catalogs is the result of testing performed on small toroidal cores, it is not always clear that these data are adequate for use in designing devices that use larger cores. These larger cores can suffer from dimensional effects such as large eddy-current losses and dimensional resonance. These dimensional effects can be modeled analytically and numerically as detailed in [14]; such modeling efforts, however, rest on the availability of reliable data for the ferrite material electrical and magnetic characteristics. In this paper, the magnetic material characterization efforts reported in [14] are explored in greater depth with a focus on the specific laboratory testing methods used to derive the material data for MnZn ferrites.

A. *Background on Core Geometry Effects*

The combination of high frequency excitation and physically large magnetic cores can result in losses and field distributions that are not encountered in lower power and lower frequency devices. This is particularly true for the ferrite core devices that are often used for such applications. These losses related to the physical dimension of the core were explored in the early history of ferrites [2] in connection with the use of large MnZn cores for accelerator magnet applications. In recent years the issues encountered in large ferrite cores have been of particular concern in high-power inductive coupling applications [13]. Such high-power applications require devices that can couple large amounts of power in a reasonable size, and this emphasis on size reduction necessitates a relatively high operating frequency. At such frequencies, ferrite materials—and MnZn ferrites in particular—are generally superior to other options such as strip or powder cores due to ferrite's inherently low losses.

While the ferrite materials themselves have relatively low losses at frequencies in the hundreds of kilohertz, specific ferrite core structures may have significantly higher losses than expected for several reasons. Flux may crowd in corners or be unevenly distributed due to uneven core cross-sectional area. This flux crowding causes higher loss hot-spots in some regions of the core, but is only rarely a significant concern. Eddy currents induced in the core can be a significant loss component for very large cores. If the induced currents are large, they shield the flux from the inner sections of the core cross-section resulting in a flux skin effect analogous to the skin effect in the conductors of windings. Finally, dimensional resonance due to the propagation of electromagnetic waves within the structure can significantly change the overall flux distribution and lead to additional losses.

B. *Standard Measurement Techniques*

The material characteristics reported in this paper are derived from a set of specially constructed toroidal cores and ferrite slabs meant to minimize geometrical effects. In contrast, standard magnetic measurements reported by manufacturers are based on tests of standard toroids—typically using a one–inch outer diameter core—tested using a relatively standard test apparatus such as the Clark Hess core characterization tester [1, 9]. Such measurements methods are convenient, provide a way to track variation in the manufacturing process, and establish a measure of relative performance between various materials.

What the standard tests do not provide is any measure of the variation that can be expected between cores of different sizes. In the best circumstance, core manufacturers would provide measured loss and permeability data for each core size they manufacture, but this extensive testing is not generally available. This paper presents some issues encountered in measurements of the material characteristics of ferrites with a particular focus on methods that are useful for eliminating the effect of core size on the measured results. These testing strategies are designed to provide the characteristics of the material itself for later use in numerical field simulations that model the effects of core size and structure on the overall device performance.

Magnetic materials are characterized from an electrical perspective by the values of electrical conductivity, magnetic permeability and dielectric constant. The following discussion illustrates how the permeability is extracted from an inductive measurement setup and the dielectric constant and conductivity are derived from a capacitive measurement.

II. PERMEABILITY

The complex permeability—whose real part is associated with the inductance of the core and whose imaginary part reflects the losses present in the core—and the magnetic loss density values for various flux density levels and excitation frequencies are extracted from measurements of the impedance of a thin toroidal core as shown in Fig. 1

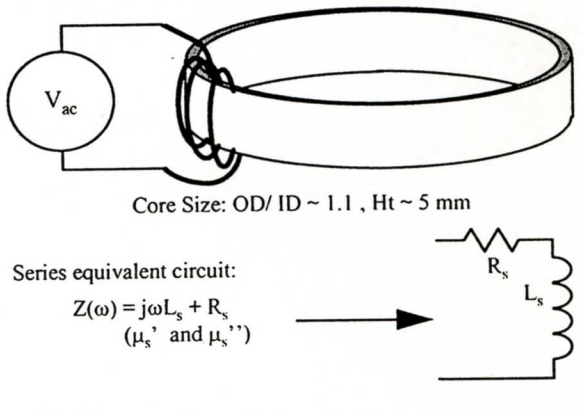

Figure 1: Core samples of MnZn ferrite used to measure magnetic and electric characteristics of the material. The thin-walled toroid ensures a uniform flux density, low thermal gradients and low eddy-current effects.

A. *Testing Set-Up*

The impedance measurement approach described in [3, 11, 17] is used in the measurements of the magnetic characteristics presented here. For the relatively low frequencies considered, the lumped element model of an inductor can be simplified to either the series R-L circuit of Fig. 2(a) or the parallel R-L combination of Fig. 2(b). In these equivalent circuit representations, all

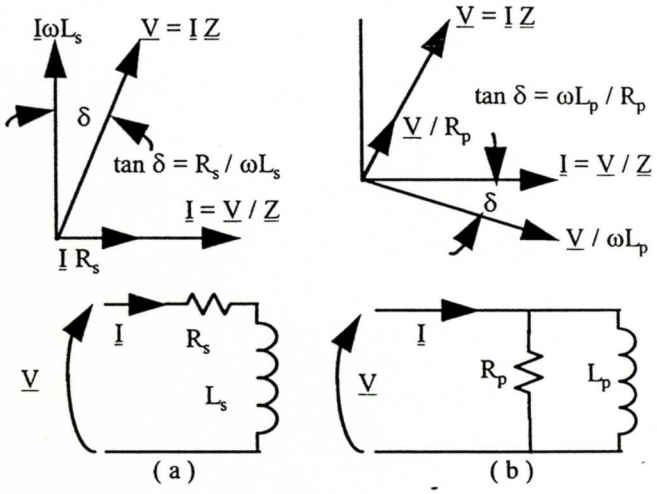

Figure 2: Lumped element equivalent circuits and the phase relationships between current and voltage for the inductor used to measure complex permeability. (a) a series RL circuit, (b) a parallel RL circuit.

of the losses in the device are combined into a single resistive element; all of the inductance—both the inductance associated with the flux in the core itself as well as the inductance of the air flux—is represented by the single inductive element. Since the losses and energy storage characteristics of the device are functions of the excitation frequency, these lumped element circuit components are generally function of ω as noted in Fig. 2.

The impedance of an N-turn inductor such as that shown in Figure 1 is used to compute the complex permeability. Figure 2 shows that the impedance of the core can be represented at any given frequency by the series combination of a resistance, R_s, and an reactance, $j\omega L_s$. These circuit component values are related to the components of the series complex permeability, μ'_{s_r} and μ''_{s_r} as,

$$R_s = \frac{\omega N^2 A_e}{\ell_e}\mu''_{s_r}\mu_o = \omega L_o \mu''_{s_r} \quad (1)$$

$$L_s = \frac{\mu_o \mu'_{s_r} N^2 A_e}{\ell_e} = L_o \mu'_{s_r} \quad (2)$$

where L_o is the air-core inductance.

The software that runs the impedance measurement system models the impedance of the device under test using the parallel circuit shown in Figure 2(b). This parallel circuit is more appropriate for determining the excitation conditions of the core since the test voltage corresponds directly to the flux value in the device under test (DUT). That is, the flux density in the core and the voltage across the parallel $R_p - L_p$ combination are directly related by the transformer equation,

$$V_{rms} = \sqrt{2}\pi N A_e B_m f \quad (3)$$

where V_{rms} and B_m are the rms value of the exciting voltage and the peak value of the sinusoidal flux density respectively. Since the voltage across the inductor in the series model is determined by the voltage divider between the resistive and reactive element, the flux density in the core is not directly related to the excitation voltage.

The parallel R-L circuit impedance is,

$$\underline{Z}_p(\omega) = \frac{1}{\frac{1}{R_p} + \frac{1}{j\omega L_p}} \tag{4}$$

where R_p and L_p represent the measured values of parallel resistance and inductance for any frequency. These circuit elements can be represented in terms of a parallel complex permeability as

$$R_p = \frac{\omega \mu_o \mu''_{p_r} N^2 A_e}{\ell_e} = \omega L_o \mu''_{p_r} \tag{5}$$

$$L_p = \frac{\mu_o \mu'_{p_r} N^2 A_e}{\ell_e} = L_o \mu'_{p_r} \tag{6}$$

The parallel complex permeability values can be determined by rearrangement of (6) and (6). However, the FEA software requires the series complex permeability as the input material characteristic, and therefore the parallel complex permeability components must be transformed to their series equivalents using the relationship,

$$\frac{1}{\mu'_s - j\mu''_s} = \frac{1}{\mu'_p} - \frac{1}{j\mu''_p} \tag{7}$$

This yields,

$$\mu'_s = \frac{\mu'_p}{1 + (\frac{\mu'_p}{\mu''_p})^2} \tag{8}$$

$$\mu''_s = \frac{\mu''_p}{1 + (\frac{\mu''_p}{\mu'_p})^2} \tag{9}$$

B. *Test Calibration*

The impedance analyzer software is designed to test a given DUT using either a constant flux density at a variety of test frequencies or a set frequency for a range of flux density values. Whichever test is chosen, the equipment must be calibrated with respect to the DUT, and this can be done in one of several ways. First, the HP4194A itself should be calibrated through the standard impedance probe calibration procedure. In this calibration step, the open circuit (0 siemens), short circuit (0 ohms) and reference impedance (50 ohms) fixtures are used to calibrate the *probe-plus-amplifier* configuration. Second, the winding resistance and stray inductance of the core can be compensated for by performing an open-circuit and short-circuit calibration in place of the DUT. The short-circuit calibration uses a winding similar to that used on the DUT but wound on a non-magnetic structure.

The calibration for the winding resistance and stray inductance is often inconsequential for the measurement of the ferrite toroids considered here since these parasitic elements are only a small fraction of the measured impedances. This is illustrated in Fig. 3 which shws the error percentage of the real and imaginary part of the measured impedance. This error percentage is defined as $\epsilon_{cal} = (A_{\text{comp}} - A_{\text{uncomp}})/A_{comp}$ where A_{comp} and A_{uncomp} are the compensated and uncompensated values of the given quantity. Figure 4 shows the measured loss density for a core with and without the calibration procedure being performed. Figures 3 and 4 show that the impedance of the winding itself is a small fraction of the total impedance; this reinforces the fact that the calibration of the winding through the short-circuit calibration is not usually a large source of error in the type of measurements presented here.

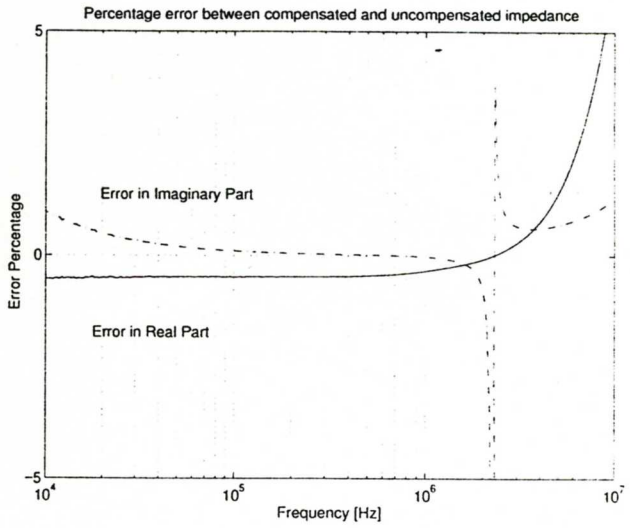

Figure 3: Measurement error vs. frequency for the real and imaginary parts of the impedance. The error is defined as the difference of the compensated and uncompensated values normalized to the compensated value.

C. *Specifications of Toroid Sample*

The geometry of the core sample is important to the accuracy of the complex permeablity values derived from the measurement. In performing such measurements of the *material* characteristics, it is important to minimize the effects that can change the losses in the core: eddy-currents, thermal gradients through the core, and flux density variations.

Commercial ferrite toroidal cores typically have a ratio of outside diameter to inside diameter in the range of 1.5 to 2.0. This means that the flux density—which varies as $1/r$ through the core cross-section—can be significantly higher on the inner edge of the core than on the outer portion of the toroid. This

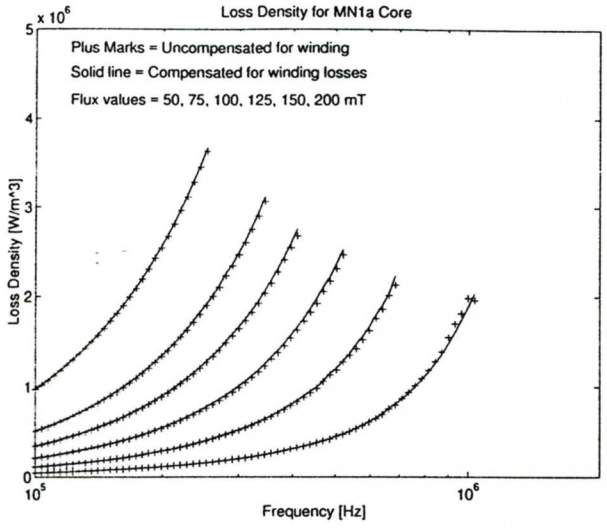

Figure 4: Plot of measured loss density of core #3 from Table 1 below with and without compensating for the winding impedance.

variation of flux density is compensated in the inductance calculations through the use of *effective* core geometries A_e, ℓ_e and V_e. These effective parameters are given [7] in terms of the core constants C_1 and C_2 as,

$$A_e = \frac{C_1}{C_2} \tag{10}$$

$$l_e = \frac{C_1^2}{C_2} \tag{11}$$

$$V_e = A_e \ell_e \tag{12}$$

where the core constants are computed for toroidal cores in terms of the core height, h, and the inner and outer radii of the core, r_o and r_i, as,

$$C_1 = \frac{2\pi}{h \ln(r_o/r_i)} \tag{13}$$

$$C_2 = \frac{2\pi(1/r_i - 1/r_o)}{h^2 \ln^3(r_o/r_i)} \tag{14}$$

In order to minimize any adverse effects that variations in flux density within the core have on the measurement of the material constants, however, it is helpful to use very thin cores that minimize the ratio of the outer diameter to the inner diameter. In the tests presented here, we use specially machined cores with OD/ID ratio values of approximately 1.1. These thin-walled samples are listed as core 1–3 in Table 1.

D. *Single-Port vs. Dual-Port Measurements*

The single port impedance probe measurement setup and calibration procedures outlined above are generally adequate for small cores without air gaps. For such devices the magnetizing current and leakage inductance are kept relatively small. However, at low frequencies the blocking capacitors of the impedance probe present significant series impedance [17], and an alternative test strategy that uses two separate windings such as shown in Figure 5 is useful. This two-winding test approach [17, 16] uses one winding to excite the core and a separate winding to sense the flux induced in the core.

There are several advantages to using separate excitation and sensing windings including the elimination of voltage drops due to winding resistance and the ability to sense the flux in several regions of the core through the use of additional voltage pick-up windings. However, error in the pickup winding, phase errors between the different probe channels and errors introduced in processing the measured data can limit the accuracy of such measurements to frequencies below the megahertz range [3]. The setup shown in Figure 5 eliminates some of these problems by using the impedance analyzer in its gain/phase mode to derive the impedance of the DUT. This setup is limited by the maximum input voltage of 2.42 V_{rms} for the impedance analyzer's test and reference channels[1]; only relatively small voltages can be sensed with such a setup, but this is not a significant restriction for measuring the small core samples of Table 1 at frequencies of approximately 10 kHz.

The low-frequency measurements obtained using the two-port test strategy are useful for determining the baseline hysteresis losses for the material. If the low-frequency losses are assumed to be due solely to hysteresis loss, then a plot of the measured losses normalized to frequency gives the residual losses (as well as any eddy current or other dimensional loss effects) for the material.

Table 1: Toroidal core geometries

Core Number	A_e	ℓ_e	V_e	OD/ID
1	1.08e-5	1.33e-1	1.44e-6	1.106
2	9.25e-6	1.18e-1	1.09e-6	1.105
3	5.06e-6	6.55e-2	3.31e-7	1.099
4	2.63e-5	2.89e-2	7.60e-7	2.259
5	4.55e-4	1.91e-1	8.69e-5	1.775
6	3.44e-4	2.78e-1	9.56e-5	1.354

E. *Thermal Gradients*

An additional issue that must be considered when measuring material characteristics is the presence of thermal gradients in the core. This is critical in ferrites since the core loss and permeability is dependent on temperature. If all sections of the

[1] The attenuators used in the single port measurement cannot be used in this case since they would place a 50 Ω load on the output of the DUT. This can be alleviated through the use of high-impedance attenuators or probes or through the use of an impedance-matching transformer.

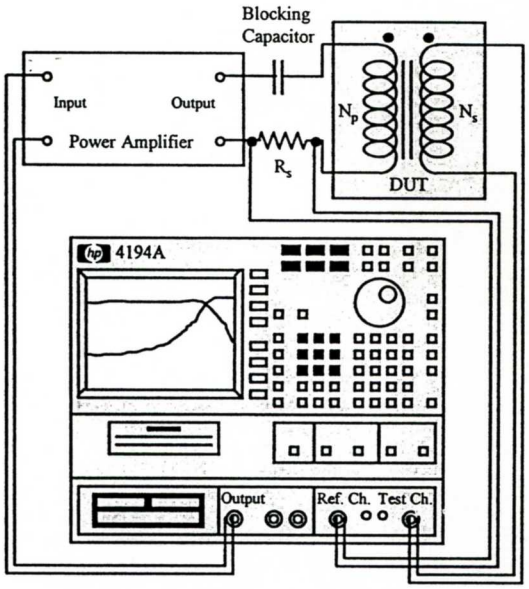

(a)

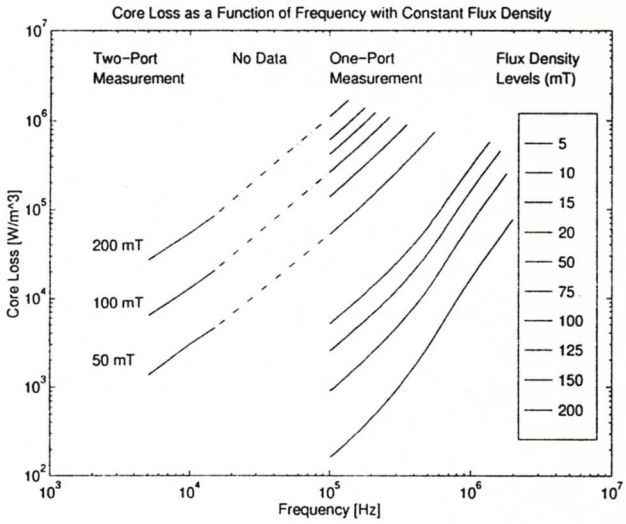

(b)

Figure 5: Two-port measurement system

core are not at the same temperature then the measurement results can be unreliable. We address this issue in two ways: (1) the use of thin cores with small values of OD/ID prevents the buildup of thermal gradients between different portions of the core; (2) the use of the impedance analyzer to excite the core for short duration at each measurement point prevents significant self-heating of the core. Finally, when testing at elevated temperatures the core is allowed to soak at the test temperature for at least 20 minutes before testing to ensure the core is isothermal.

F. *Winding Arrangement*

The windings on the sample cores should ideally wrap fully around the circumference of the toroid. This uniform winding reduces the amount of flux that leaves the core, and thus provides for a more uniform flux density. However, the maximum number of turns allowed on the core is limited by the restrictions on the maximum value of the test voltage. When this is the case, a multistranded winding with fewer turns can be used to provide the desired uniform flux density. Figure 6 shows how a multistranded winding with four conductors per turn results in a fully wound structure.

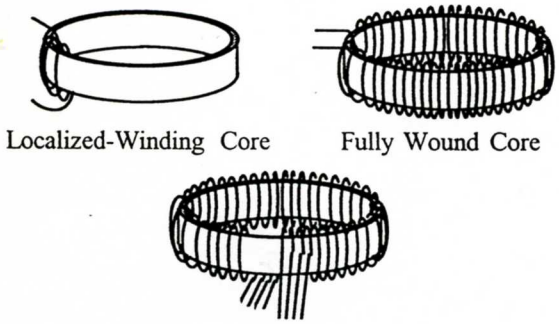

Figure 6: Winding arrangements for thin toroidal cores.

While the use of a fully-wound device—whether it be wound with only a small number of multi-stranded turns or with many single-strand turns—provides a more uniform flux density, it is not well documented what impact a "non-ideal" winding has on the measured characteristics of the material. For high-permeability ferrite cores, the difference in flux density in the core due to leakage is relatively small. This is illustrated in Figure 7(a) which shows the results of an FEA simulation of the flux in core #1 from Table 1. The graphs in Figure 7 give the ratio of the net flux in the core at locations 2, 3, and 4 relative to the flux that links the excitation winding (point 1). The ratio $\beta = \Phi_2/\Phi_1 = \Phi_4/\Phi_1$ gives the percentage of the source flux that links points 2 and 4; the ratio $\zeta = \Phi_3/\Phi_1$ gives the percentage of the source flux that reaches the opposite side of the toroid (point 3). The flux that links all parts of the core is approximately 90% of the source flux for core permeability val-

ues above 1000. When the relative permeability is 3000, approximately 97% of the flux remains within the core. Fig. 7(b) shows that the loss density values measured using the multi-stranded six-turn winding correlate well with the fully-wound 25-turn winding; a six-turn winding that is localized in only a small section of the core, however, underestimates the loss in the core by approximately 20 percent. The results in Fig. 7(a) and (b) show that while the location of the winding may introduce only a small difference in flux density in the different parts of the core (on the order of 5–10%), this relatively small change in flux density can introduce a significant error in the measured losses since the loss density is a string function of the flux density; typically, the loss density in ferrite depends on the flux density to the power of 2.2 to 2.5 which means a 10% error in flux leads to a 20–25% error in loss.

G. *Effects of Core Size*

The effects of core size on the apparent loss density and permeability of a given material is illustrated by comparing the values measured on the thin toroidal cores (#2–#3) to the results obtained for the large toroidal cores (#5–#6). Figure 8(a) shows the measured series permeability (real part) as a function of frequency for the different toroidal core structures. The flux density in these tests is 15 mT. For all of the larger cores, the bandwidth of the apparent permeability is less than that of the thin toroid; the largest cores have the lowest roll-off frequency since they suffer the most significant dimensional effects.

Figure 8(b) shows the core loss density of each of the cores for a flux density of 15 mT. Here again, the larger cores have more significant changes from the baseline material data, and in all cases the loss density in the core is higher than predicted by the published material data.

III. Electric Material Characteristics

A. *Testing Setup*

The measurement of magnetic material characteristics described in the previous section follows from the assumption that the thin toroidal core is a good inductor with uniform magnetic flux density. This section presents measurements of the electrical conductivity and dielectric constant of these ferrites based on the the assumption that thin plates of material are good capacitors with uniform electric flux density.

The electrical measurements use the parallel-plate capacitor structure shown in Figure 9. The capacitive admittance of each thin plate is measured using an HP4194A impedance analyzer with the HP16451B dielectric test fixture. The real part of the measured admittance is used to derive the frequency dependent conductivity of the core and the measured capacitive reactance gives the core permittivity spectrum. The calibration

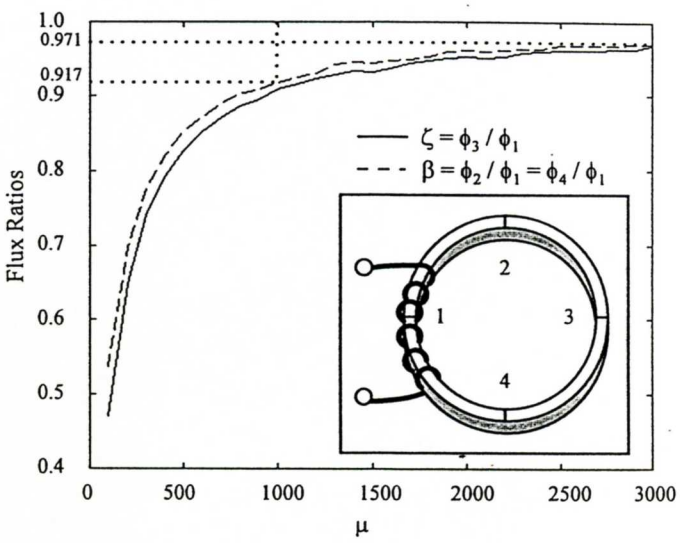

(a)

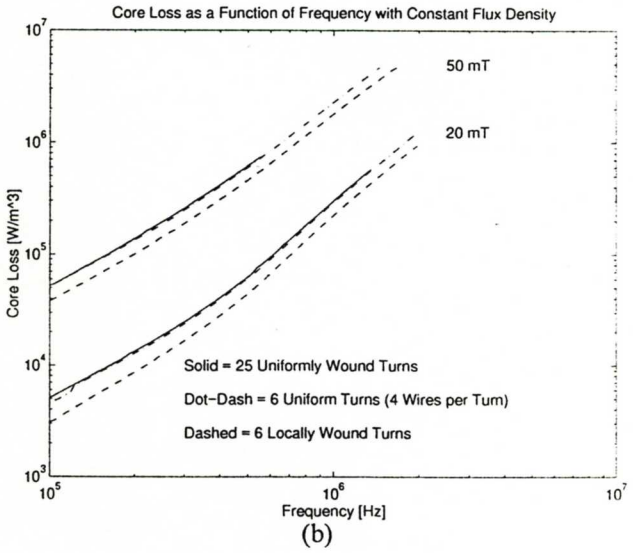

(b)

Figure 7: Comparison of flux density for different winding arrangements on toroid sample #1. (a) Ratio of flux density at different locations within the core as a function of the core permeability. (b) Measured loss density for six single-strand turns concentrated in one section of the core, six multi-strand turns that wrap around the entire circumference, and 25 single-strand turns that wrap around the circumference.

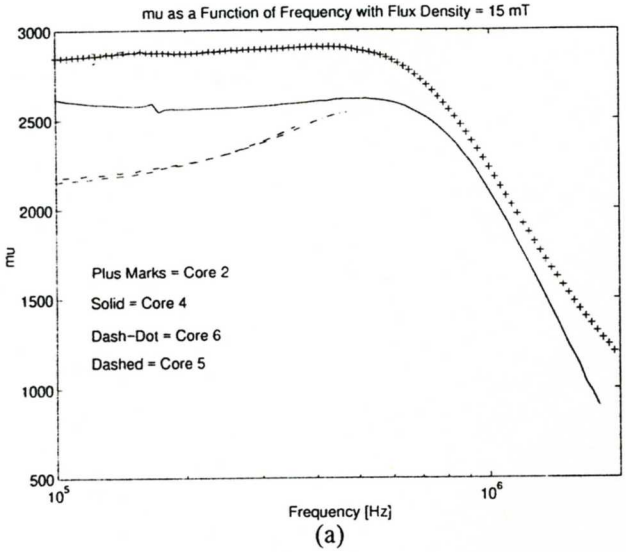

(a)

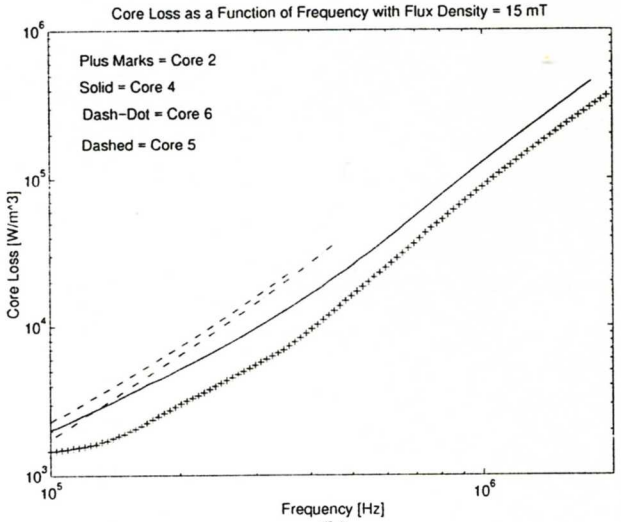

(b)

Figure 8: Tests of different size B2 material cores. (a) Series permeability (real part) vs. frequency at 15 mT. (b) Core loss density at 15 mT.

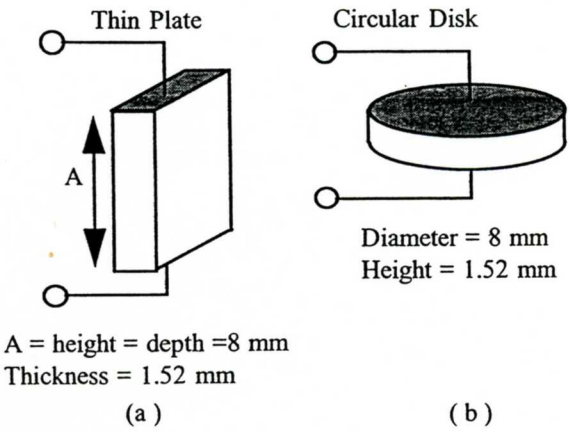

Figure 9: Core samples of MnZn ferrite used to measure electrical conductivity and dielectric constant. The thin-walled ferrite slabs in (a) ensure a uniform electric flux density as compared with the relatively large diameter disk samples in (b).

procedures used in this test procedure are those outlined in the HP16451B manual [6]. The key aspects of this calibration procedure as well as the sample preparation and size restrictions are the main issues of concern in measuring the ferrite electrical characteristics. These issues are discussed separately in the following paragraphs.

B. *Ferrite Samples for Electrical Testing*

The HP16451B test fixture has four different electrodes that can be used for measuring different types of samples: one large and one small electrode for testing samples with thin-film electrodes attached to them and one large and one small electrode for testing samples without thin-film electrodes. Each of the HP16451B's electrodes provides both a center contact (the guarded electrode) and an outer ring contact (the guard electrode); the guard electrode is intended to minimize the effects of fringing near the edge of the guarded electrode. The dimensions of the samples that each electrode can test are listed in Table 2

Table 2: Sizes of the samples that can be tested using the different electrodes of the HP16451B Dielectric Tester

Electrode Number	Type	Min. Sample Diam. [mm]	Max. Sample Diam. [mm]
A	Contact	40	56
B	Thin Film	10	56
C	Contact	56	–
D	Thin-Film	20	50

1) *Fringing Effects and Guard Electrodes:* The ferrite samples tested here do not generally meet the size restrictions listed in Table 2, which challenges the reliability of the results obtained using these samples. We justify the validity of the measured data based on the assumption that the high dielectric constant of MnZn ferrite materials makes the fringing of the electric field near the edges of the samples relatively unimportant. This assumption is equivalent to the assumption that the high permeability of the ferrite allows us to treat the flux density as close to uniform in the core when testing the magnetic characteristics on the thin toroidal samples. Under this assumption of uniform electric flux, the measured capacitance for the geometry of the samples used is given by the ideal parallel-plate capacitance equation.

2) *Sample Size:* In the standard calculation of capacitance based on the ideal parallel-plate capacitance equation, the two plates that bound the material under consideration are assumed to be equipotential surfaces. At DC this is certainly the case since the conductive plates cannot support a voltage difference under static conditions. However, under AC excitation it is possible that the conductive plates are not equipotential. This is particularly the case when the dimension of the sample under test is a significant fraction of the electromagnetic wavelength in the ferrite material at the excitation frequency. In other words, if the diameter of the sample used for testing the dielectric nature of the ferrite is large, then what is measured is not the inherent complex dielectric constant of the material but rather the *effective* dielectric constant. In order to measure the true material constant, therefore, the sample size should be a small fraction of the wavelength over the entire frequency range of interest.

This dimensional effect is illustrated in the graphs of measured conductivity and real dielectric constant Figure C. below. In these plots, the measured values from samples with small cross-sectional dimensions are compared to those measured on samples with relatively large diameters. The fact that the larger samples show a resonant behavior at relatively low frequencies indicates that the samples are not sufficiently thin to permit the measurement of the true material constants for these frequencies. The results in Figure C. confirm the results presented by Brockman, et al. in [2] where the apparent dielectric constant for a 0.127 cm. thick MnZn ferrite sample is compared to a sample approximately ten times thicker. The samples that we take as giving the "true" result in Figure C. are approximately the same thickness as those used in [2].

3) *Surface Preparation and Plating:* The tests of the ferrite's electrical characteristics minimize the contact resistance to the ferrite by first plating the samples with a thin layer of metal. It is possible to then solder leads to the metallization layers and test the samples as one would test any capacitor. However, the use of the dielectric test fixture on the impedance analyzer simplifies this process since there is no need to solder leads to the samples; all of the test results presented here use this "leadless" testing approach.

In order to achieve a good contact for the plating material it is important to prepare the samples correctly. The test surfaces of the samples are first lightly wet-sanded to remove surface contamination and to provide a smooth surface for electrode plating. This is followed by ultrasonic cleaning in acetone and isopropyl alcohol to remove organic contaminants from the surface; this improves the attachment of the plating material. The samples are then taped so that only the surfaces that should have metal plating deposited on them are exposed, and finally metallic contacts are deposited through vacuum sputtering process. For the samples tested here the plating metal is platinum.

C. *Results*

Figure C. shows the electrical conductivity and relative dielectric constant. Note that the dielectric constant of MnZn ferrite is extremely high, on the order of 100,000. The conductivity is small—approximately 0.2 S/m—at low frequencies but increases an order of magnitude over the frequency range tested. This means that any calculation of eddy-current losses in the core that are based on the DC conductivity will be inaccurate at higher frequencies. Note also in Figure C. that the dielectric constant decreases with frequency but that the value at one megahertz is still quite high; this means that the critical size for the onset of dimensional resonance becomes somewhat larger as frequency increases, however this change is rather slight.

IV. Conclusions

The standard test data available from manufacturers for various ferrite materials are generally adequate for many standard designs. When it is important to have independent confirmation of such data or when additional information is required, however, it is critical that the testing strategies be carefully considered. This paper illustrtes some—but by no means all—of the issues that must be addressed when attempting to extract the intrinsic performance data for a given material. In addition, the impact that the size of the toroidal core or dielectric slab used in the test has on the measured parameters reinforces the need for care in the application of data measured on one device to the calculation of the performance of devices of different size or shape.

References

[1] L.M. Bosley, "Data sheets provide clues for optimizing selection of SMPS ferrite core material," *Powerconversion and Intelligent Motion*, 1993, p. 13-15.

[2] F.G. Brockman, P.H. Dowling and W.G. Steneck, "Dimensional Effects Resulting from a High Dielectric Constant Found in a

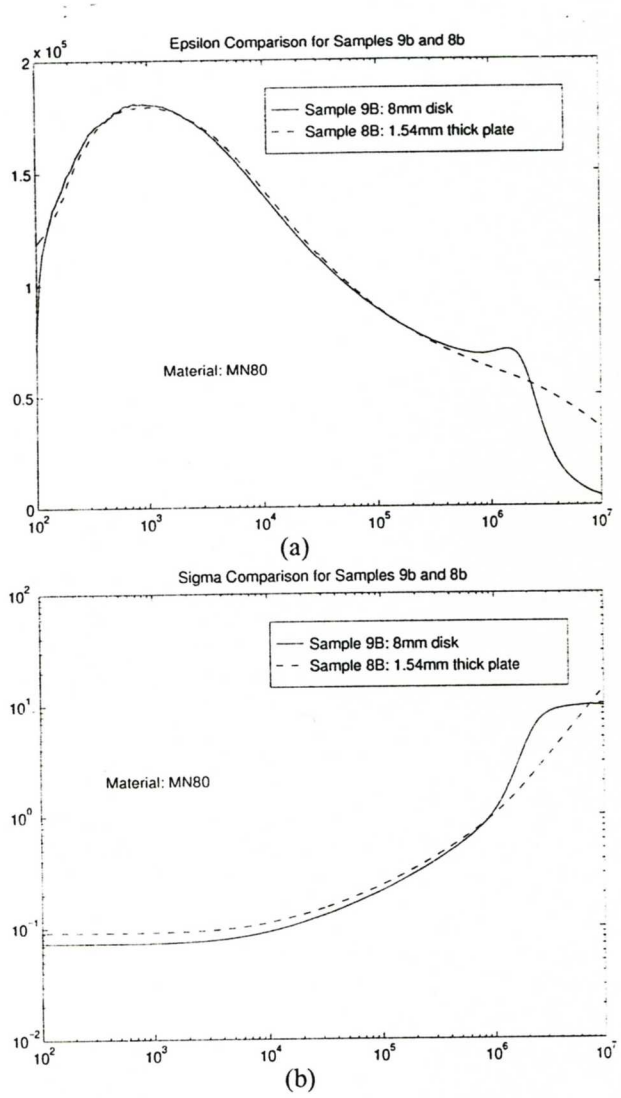

Figure 10: Electrical characteristics, ϵ and σ, vs. frequency for B2 MnZn ferrite material.

Ferromagnetic Ferrite", *Physical Review, Vol. 77, NO. 1*, January, 1950.

[3] P.M. Gradzski, *Core Loss Characterization and Design Optimization of High- Frequency Power Ferrite Devices in Power Electronics Applications*, Ph.D. Dissertation, Virginia Polytechnic Institute and State University, 1992.

[4] C. Guillaud, "The properties of Manganese-Zinc Ferrites and the Physical Processes Governing Them", *Proceedings of the IEE, Suppl. 5*, 1957, p. 165-178.

[5] W. H. Hayt, *Engineering Electromagnetics*, 5th Ed., McGraw-Hill, New York, 1989.

[6] "HP 16451B Dielectric Test Fixture: Operation and Service Manual,", HP Part No. 16451-90000, 3rd Ed., 1993.

[7] "Calculation of the effective parameters of magnetic piece parts," *International Electrotechnical Commission, Pub. 205*, Geneva, 1966.

[8] C.G. Koops, "On the Dispersion of Resistivity and Dielectric Constant of Some Semiconductors at Audio Frequencies", *Physical Review,Vol. 83 NO. 1*, 1951, p. 121-124.

[9] MMPA, *Magnetic Materials Producers Association Ferrite Users Guide*, 1992.

[10] E. Otsuki, S.Y. Otsuka, K. Shoji and T. Sato, "Microstructure and Physical Properties of Mn-Zn Ferrites for High-Frequency Power Supplies", *Journal of Applied Physics,Vol. 69 NO. 8*, 1991, p. 5942-5944.

[11] P. Han, "Characterization of MnZn Ferrite Materials and Finite Element Method for MnZn Ferrite Core Loss Calculations," Master's Thesis, Virginia Polytechnic Institute and State University, 1995.

[12] D. Polder, "Ferrite Materials", *Proceedings of the IEE,Vol. 97(Part II)*, 1950, p. 246-256.

[13] R. Severns, E. Yeow, G. Woody, J. Hall and J. Hayes, "An Ultra-Compact Transformer for a 100 W To 120 kW Inductive Coupler for Electric Vehicle Battery Charging", *IEEE Applied Power Electronics Conference Conference Record*, 1996, p. 32-38.

[14] G. R. Skutt and F. C. Lee, "Characterization of Dimensional Effects in Ferrite-Core Magnetic Devices", *IEEE Power Electronics Specialists Conference Record*, 1996, p. ???.

[15] E.C. Snelling, *Soft Ferrites*, 2nd Ed., Butterworths, London, 1988.

[16] V. J. Thottuvelil, T.G. Wilson, and H. A. Owen, Jr.,"High-frequency measurement techniques for magnetic cores", *IEEE Transactions on Power Electronics*, vol. 5, num. 1,p. 41-53, 1990.

[17] J. Zhang, G. R. Skutt and F. C. Lee,"Some Practical Issues Related to Core Loss Measurement Using Impedance Analyzer", *IEEE Applied Power Electronics Conference Record*, 1995, p. 547-554.